DESY 96–172
INLO-PUB-17/96
WUE-ITP-96-017
August 1996

Theoretical Uncertainties in the QCD Evolution of Structure Functions and their Impact on $\alpha_s(M_Z^2)$

J. Blümlein, S. Riemersma

DESY–Zeuthen
Platanenallee 6, D–15735 Zeuthen, Germany

W.L. van Neerven

Instituut Lorentz, Rijksuniversiteit Leiden,
PO Box 9506, 2300 RA Leiden, The Netherlands

A. Vogt

Institut für Theoretische Physik, Universität Würzburg
Am Hubland, D–97074 Würzburg, Germany

Abstract

The differences are discussed between various next-to-leading order prescriptions for the QCD evolution of parton densities and structure functions. Their quantitative impact is understood to an accuracy of 0.02%. The uncertainties due to the freedom to choose the renormalization and factorization scales are studied. The quantitative consequences of the different uncertainties on the extraction of the strong coupling constant α_s from scaling violations in deep–inelastic scattering are estimated for the kinematic regime accessible at HERA.

To appear in the Proceedings of the 1996 Zeuthen Workshop on Elementary Particle Theory: QCD and QED in Higher Orders, Rheinsberg, Germany, April 1996, Nucl. Phys. **B** (Proc. Suppl.).

Theoretical Uncertainties in the QCD Evolution of Structure Functions and their Impact on $\alpha_s(M_Z^2)$*

J. Blümlein [a], S. Riemersma [a], W.L. van Neerven [b], and A. Vogt [c]

[a]DESY–Zeuthen, Platanenallee 6, D–15735 Zeuthen, Germany

[b]Instituut Lorentz, Rijksuniversiteit Leiden, PO Box 9506, 2300 RA Leiden, The Netherlands

[c]Institut für Theoretische Physik, Universität Würzburg, Am Hubland, D–97074 Würzburg, Germany

The differences are discussed between various next-to-leading order prescriptions for the QCD evolution of parton densities and structure functions. Their quantitative impact is understood to an accuracy of 0.02%. The uncertainties due to the freedom to choose the renormalization and factorization scales are studied. The quantitative consequences of the different uncertainties on the extraction of the strong coupling constant α_s from scaling violations in deep–inelastic scattering are estimated for the kinematic regime accessible at HERA.

1. Introduction

Deeply inelastic scattering (DIS) has a long and successful history in the discovery and analysis of the substructure of the nucleon. It provides one of the cleanest tests of QCD. With the advent of HERA, the kinematic range has been extended to Q^2 values up to about $10^4\,\mathrm{GeV}^2$. Moreover in the Bjorken–variable x, the range down to values of $x \simeq 10^{-4}$ is now probed in the deep–inelastic regime. This extended kinematic coverage allows for detailed measurements of the scaling violations of the structure function $F_2(x, Q^2)$ and, consequently, of the strong coupling constant α_s. The statistical and systematic experimental errors for such analyses have been estimated in refs. [1,2].

The determination of α_s in analyses of DIS data from high statistics experiments relies on perturbative QCD expansions, implemented in complicated fitting procedures. Presently the necessary theoretical ingredients are fully known only up to next-to-leading order (NLO). In this paper, we analyze the theoretical ambiguities arising at this level of accuracy, and study their implications for the extraction of $\alpha_s(M_Z^2)$ from the scaling violation of the structure function F_2.

The paper is organized as follows. In Section 2 we give a detailed discussion of the various approximations used in different solutions of the evolution equations. We examine their quantitative impact on the predicted scaling violations of the parton densities and structure functions. Section 3 is devoted to the uncertainties originating from the choice of the renormalization and mass factorization scales at this order of the perturbative expansion. The implications of all these effects for the theoretical error $\Delta\alpha_s(M_Z^2)$ from QCD analyses of DIS scaling violations in the kinematic range at HERA are presented in Section 4. Section 5 contains the conclusions.

2. Structure function evolution in NLO

In this section the details of various representations of the evolution equations in NLO and the renormalization group equation determining α_s are compared. To keep the notation as compact and transparent as possible, the evolution equations will be written in a generic manner, which covers the non–singlet equations as well as the coupled singlet quark and gluon evolution equations. Explicit solutions written down in Sections 2.2 and 2.3 will apply literally only to the non–singlet cases. A numerical comparison of the different prescriptions is performed in Section 2.4.

*Talk presented by S. Riemersma

2.1. Evolution equations for parton densities and $\alpha_s(Q^2)$

The evolution equations for the (twist-2) parton distributions $f(x, M^2)$ of the nucleon are given by

$$\frac{\partial f(x,M^2)}{\partial \ln M^2} = \left[a_s(M^2)\, P_0(x) + a_s^2(M^2)\, P_1(x) + O(a_s^3)\right] \otimes f(x,M^2)\,. \quad (1)$$

As usual x stands for the nucleon's momentum fraction carried by the partons, and $\otimes$ denotes the Mellin convolution,

$$A(x) \otimes B(x) = \int_x^1 \frac{dy}{y}\, A(y)\, B\left(\frac{x}{y}\right)\,. \quad (2)$$

M represents the mass factorization scale. In eq. (1) we have already inserted the perturbative expansion of the splitting functions $P(x, M^2)$ in powers of the strong coupling constant $\alpha_s(M^2) \equiv 4\pi a_s(M^2)$. Only the first two expansion coefficients $P_0(x)$ and $P_1(x)$ are completely known so far. Hence the solution of the evolution equations is presently possible up to NLO.

To this accuracy the scale dependence of $a_s(R^2)$ is governed by

$$\frac{\partial\, a_s(R^2)}{\partial \ln R^2} = -\beta_0 a_s^2(R^2) - \beta_1 a_s^3(R^2) + O(a_s^4)\,, \quad (3)$$

with the first two (scheme independent) coefficients of the QCD beta function given by $\beta_0 = 11 - 2N_f/3$ and $\beta_1 = 102 - 38N_f/3$. Here N_f denotes the number of quark flavours. As already indicated in eq. (1), the renormalization scale R is identified with the factorization scale in this section, $R = M$. For the case that R and M are chosen to be unequal see Section 3.

Like the solution of the parton evolution equation (1), discussed in detail below, also the NLO running of a_s can be treated in several ways, differing beyond the accuracy of the present approximation. First, eq. (3) can be simply solved by numerical iteration starting from a reference scale R_0, or equivalently by using its integrated implicit form

$$\frac{1}{a_s(R^2)} = \frac{1}{a_s(R_0^2)} - \beta_0 \ln\left(\frac{R^2}{R_0^2}\right) + \frac{\beta_1}{\beta_0} \ln\left\{\frac{a_s(R^2)[\beta_0 + \beta_1 a_s(R_0^2)]}{a_s(R_0^2)[\beta_0 + \beta_1 a_s(R^2)]}\right\}. \quad (4)$$

Second, since in lowest order $1/a_s \sim \ln(R^2/R_0^2)$, one can treat eq. (3) in the sense of a power expansion in $1/\ln(R^2/R_0^2)$, and keep only the powers to which the terms in eq. (3) beyond β_1 do not contribute. Introducing the QCD scale parameter Λ instead of the reference value $a_s(R_0^2)$, the result can be written as

$$a_s(R^2) = \frac{1}{\beta_0 \ln(R^2/\Lambda^2)} - \frac{\beta_1}{\beta_0^3} \frac{\ln\left[\ln(R^2/\Lambda^2)\right]}{\ln^2(R^2/\Lambda^2)} + O\left(\ln^{-3}(R^2/\Lambda^2)\right)\,. \quad (5)$$

Both these treatments, as well as slightly different analytic approximations [3], e.g. by truncating in $1/a_s$ instead of a_s as in eq. (5), have been widely used in the context of parton evolution.

Let us now return to the evolution equation (1). This system of coupled integro–differential equations has been treated in various manners. Aside from expansions in orthogonal polynomials [4], which will not be discussed here, the principal options are to solve these equations in x-space or to consider their transformation using Mellin-N moments,

$$A^N \equiv \int_0^1 dx\, x^{N-1} A(x)\,. \quad (6)$$

In the latter case the convolution (2) reduces to the product

$$[A(x) \otimes B(x)]^N = A^N\, B^N\,, \quad (7)$$

and eq. (1) becomes a system of ordinary differential equations at fixed N.

In many analyses, eq. (1) has been solved numerically in x-space, see e.g. [5]–[7], without further reference to the power–series structure in a_s. We will denote this approach, which is a direct solution of the renormalization group equations in the case of mass factorization, as prescription **(A)** in the numerical comparisons in Section 2.4. On the other hand, the transformation of the evolution equations to N-space [8,9] allows for further analytic developments to which we now turn.

2.2. Analytic solutions and approximations

The first step towards an analytic solution of the evolution equations is to rewrite eq. (1) in terms

of a_s:

$$\frac{\partial f^N(a_s)}{\partial a_s} = -\frac{a_s P_0^N + a_s^2 P_1^N + O(a_s^3)}{\beta_0 a_s^2 + \beta_1 a_s^3 + O(a_s^4)} f^N(a_s)\,. \quad (8)$$

To simplify the notation, the argument M^2 of a_s is suppressed throughout this section. This formulation is still fully equivalent to eq. (1) in combination with eq. (4). The analytic solution of eq. (8), which is possible in a closed form for the non–singlet cases, or a numerical iterative treatment, can be used to cross-check the numerical accuracy of concrete x- and N-space implementations, see ref. [10].

Expanding the r.h.s. of eq. (8) into a power series in a_s, one arrives at

$$\frac{\partial f^N(a_s)}{\partial a_s} = \quad (9)$$
$$-\frac{1}{\beta_0 a_s}\left[P_0^N + a_s(P_1^N - \frac{\beta_1}{\beta_0}P_0^N) + O(a_s^2)\right] f^N(a_s)\,.$$

The derivation of eq. (9) consists of two steps: first one assumes that the beta function is truncated for $1/a_s$ [and not for a_s as in eq. (3)], which is of course equivalent to the order considered. Then the a_s^2 term arising in the square bracket is discarded, since at the same order in a_s also the presently unknown next-to-next-to-leading order (NNLO) splitting functions P_2^N enter. Hence this term is beyond the order being considered here. The direct solution of eq. (9) will be referred to as prescription **(B)** [11] in the numerical comparisons below.

Keeping the power–series character of the evolution equations, the final step of the solution then leads to

$$f^N(a_s) = \left[1 - \frac{a_s - a_0}{\beta_0}\left(P_1^N - \frac{\beta_1}{\beta_0}P_0^N\right) + O(a_s^2)\right] \cdot \left(\frac{a_0}{a_s}\right)^{P_0^N/\beta_0} f^N(a_0) \quad (10)$$

in the non–singlet cases, with $a_0 \equiv a_s(M_0^2)$. Here M_0 is the reference scale at which the non–perturbative initial distributions are specified. With respect to the a_s expansion, the notationally more involved singlet–matrix solution behaves as eq. (10), see ref. [12]. As compared to this final result, an iterative solution of eq. (9) generates also higher powers of the P_1^N, the contribution of which is again beyond NLO in the sense of an expansion in powers of a_s. In Section 2.4, we will refer to the solution (10), which has practically been employed, for example, in refs. [8,9], as prescription **(C)**.

The Mellin–moment technique is a very powerful tool, allowing the implementation of various kinds of approximations. As we will mainly rely upon this method in our subsequent numerical work, a short reminder about the transformation of the results back to x-space is in order. The inverse Mellin transformation is performed by a contour integral in the complex N-plane,

$$f(x, a_s) = \frac{1}{\pi}\int_0^\infty dz\, \mathrm{Im}\left[e^{i\phi} x^{-C} f^{N=C}(a_s)\right], \quad (11)$$

where $C = c + ze^{i\phi}$. Here all functions f^N encountered satisfy $(f^N)^* = f^{N^*}$. The parameter c is chosen about one to two units to the right of the rightmost singularity of f^N – at $N = 1\,(0)$ for singlet (non–singlet) cases. All singularities are situated on the real axis for the NLO evolution, and $\phi \approx 3\pi/4$ [9] can be safely used even down to extremely low x. The choice of $\phi > \pi/2$ leads to a faster convergence of the integral (11) as $z \to \infty$. Using a chain of Gauss quadratures, a numerical accuracy better than 10^{-5} is easily achieved.

2.3. Structure function evolution near Q_0^2

The structure function F_2 is obtained, for $M^2 = R^2 = Q^2$, from the (anti-) quark and gluon densities f_q and f_g considered in the previous sections by

$$F_2(x, Q^2) = \sum_{i=q,g} c_i[x, a_s(Q^2)] \otimes f_i(x, Q^2)\,. \quad (12)$$

Here $c_{q,g}[x, a_s(Q^2)]$ denote the NLO coefficient functions for quarks and gluons

$$c_i[x, a_s(Q^2)] = c_{0,i}\delta_{iq}\,\delta(1-x) + a_s(Q^2)\,c_{1,i}(x)\,, \quad (13)$$

where we identify the factorization scale M by setting $M^2 = Q^2$. If Q^2 is not too far from the reference scale Q_0^2, i.e. if the evolution distance

$L = \ln(Q^2/Q_0^2)$ is small, one may Taylor expand eq. (12) around Q_0^2. In this way $F_2(x,Q^2)$ can be expressed in terms of L, the expansion coefficients of the coefficient and splitting functions, $c_i(x)$ and $P_{kl}(x)$, the parton densities $f_i(x,Q_0^2) \equiv f_{i,0}(x)$, and the strong coupling $a_s(Q_0^2) \equiv a_0$ at the initial scale.

The explicit result for this case will also be given for the notationally simpler non–singlet structure functions only. We will again switch to Mellin moments below. The approximation under consideration is most easily derived directly from eqs. (1) and (3) without reference to their solutions discussed above. First the a_s-equation (3) is solved up to orders a_0^3 and L^2, resulting in

$$a_s(Q^2) \simeq a_0 - a_0^2\beta_0 L - a_0^3\beta_1 L + a_0^3\beta_0^2 L^2 \,. \quad (14)$$

The expansion of the r.h.s. of eq. (12) in connection with eq. (1) is then, including terms up to $O(a_0^2)$ and $O(L^2)$, given by

$$\begin{aligned} F^N(Q^2) \;\simeq\; & \Big\{1 + a_0[c_{1,q}^N + P_0^N L] \\ & + a_0^2\Big[(P_1^N + P_0^N c_{1,q}^N - \beta_0 c_{1,q}^N)L \\ & + \frac{1}{2}([P_0^N]^2 - \beta_0 P_0^N)L^2\Big]\Big\} f_0^N \,. \end{aligned} \quad (15)$$

One may express this solution in terms of the coefficient function to order a_s^2, $C_q(a_0, Q^2/Q_0^2)$ [13] as

$$\begin{aligned} F^N(Q^2) \;\simeq\; & \Big\{(1 + a_0\, c_{1,q}^N) + \Big[C_q^N(a_0, Q^2/Q_0^2) \\ & - C_q^N(a_0,1)\Big]\Big\} f_0^N \,. \end{aligned} \quad (16)$$

Here the general form of the coefficient function

$$\begin{aligned} C_q^N(a_s, Q^2/M^2) \;&=\; c_{0,q} + a_s C_{1,q}^N(Q^2/M^2) \\ &+\; a_s^2 C_{2,q}^N(Q^2/M^2) + O(a_s^3) \end{aligned} \quad (17)$$

was used choosing $M^2 = Q_0^2$. The local representation (15) of the structure function evolution will be denoted as prescription **(D)** [14] in the discussion below.

2.4. Numerical comparisons

We now turn to the comparisons of the numerical results obtained by the prescriptions **(A)**–**(D)** defined in the previous sections. All these versions are equivalent to NLO. Their comparison gives information about the uncertainty induced at the level of possible approximations. The uncertainties due to different choices of the renormalization and factorization scales are discussed in Section 3.

The results will be shown for initial distributions which, although representing a somewhat simplified input, incorporate all features relevant to this study in a sufficiently realistic way. Specifically, we take in the $\overline{\rm MS}$ factorization scheme at $M_0^2 = 4$ GeV^2:

$$\begin{aligned} xu_v &= A_u x^{0.5}(1-x)^3, \; xd_v = A_d x^{0.5}(1-x)^4, \\ xS &= \Sigma - xu_v - xd_v \;\; = A_S x^{-0.2}(1-x)^7, \\ xg &= A_g x^{-0.2}(1-x)^5, \; xc = x\bar{c} = 0 \,. \end{aligned} \quad (18)$$

The evolution is performed for four massless flavours, using $\Lambda_{\overline{\rm MS}}(N_f = 4) = 250$ MeV in eq. (5). The SU(3)–symmetric sea is assumed to carry 15% of the nucleon's momentum at the input scale, and the remaining coefficients are fixed by sum rules. Also the results on F_2 will be shown employing $M^2 = R^2 = Q^2$. The massless charm evolution does not yield a correct representation of $F_2^{c\overline{c}}(x,Q^2)$. However, the conclusions of this investigation are not substantially affected by this simplification.

In Figure 1 the singlet quark and gluon densities obtained from the solutions **(A)**–**(C)** are compared, after an evolution to $M^2 = 100$ GeV^2 and 10^4 GeV^2. To display the differences clearly, the curves have been normalized to the values obtained for case **(C)**. Between the input scale and the highest scale considered in the figure, $x\Sigma$ and xg increase (decrease) by more than an order of magnitude at very low (high) values of x, respectively.

The difference between the results based on eq. (9), **(B)** and **(C)**, is very small for $10^{-3} < x < 0.9$, and reaches at most the order of 1% for smaller x. This small difference is due to the iterated P_1 terms in the solution of eq. (9). On the other hand, the deviations of the evolution **(A)** based upon eq. (1) from these results are rather large. These offsets are not related to any numer-

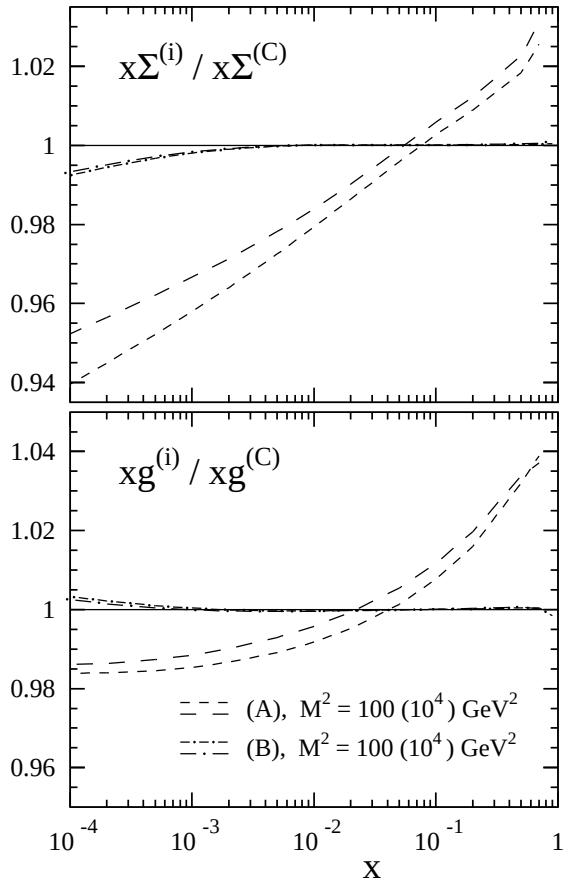

Figure 1: A comparison of the singlet quark and gluon densities, $x\Sigma$ and xg, as evolved using the prescriptions **(A, B)** discussed in the text, normalized to **(C)** for the initial conditions (18). The results are displayed at two representative choices of the factorization and renormalization scale M.

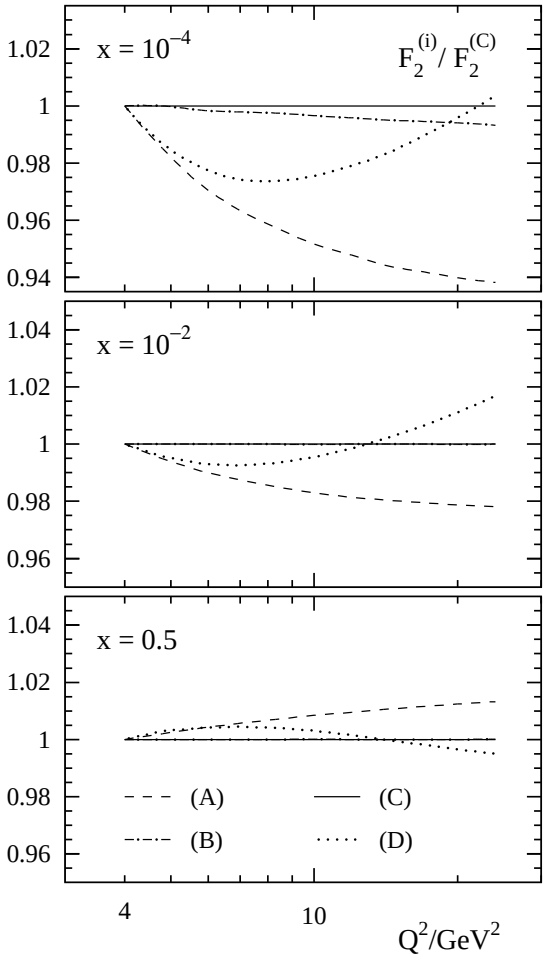

Figure 2: A comparison of the Q^2 evolutions of the proton structure function $F_2(x, Q^2)$ as obtained using the prescriptions **(A, B, D)**, normalized to **(C)** close to the reference scale $Q_0^2 = 4\,\mathrm{GeV}^2$.

ical inaccuracies, since those are under control to the level of 0.02% [10]. Instead these differences are due to both of the two expansion steps discussed below eq. (9), with the first one, the re–expansion of the beta function, being somewhat more important numerically. As will be shown in Section 4, these differences in F_2 result in a shift of $\alpha_s(M_Z^2)$ by 0.003 under the conditions at HERA.

Figure 2 shows how the offset between the solutions **(A)** and **(B,C)** develops, for three typical values of x, with increasing Q^2 in the structure function F_2. The result of the local representation **(D)**, representing an expansion valid for $L = \ln(Q^2/Q_0^2) \ll 1$, is also given here. For small values of L it agrees with scheme **(A)**. The figure indicates that the difference, observed in the previous comparison, builds up very quickly in the vicinity of Q_0^2, and then stays at about the same level above $Q^2 \approx 20\ \mathrm{GeV}^2$. This behaviour is readily explained by the large size of α_s at scales around 4 GeV^2: α_s^2 changes by almost a factor of two between 4 and 20 GeV^2.

3. Renormalization and Factorization Scale Uncertainties

The renormalization scale dependence of non-singlet parton densities f^N is determined by

$$\frac{\partial f^N(M^2,R^2)}{\partial \ln M^2} = a_s(R^2)\left[P_0^N + a_s(R^2)P_1^N + a_s(R^2)\beta_0 P_0^N \ln\left(\frac{R^2}{M^2}\right)\right] f^N(M^2,R^2)\,. \quad (19)$$

Here the values of a_s at the factorization scale M^2 and renormalization scale R^2 are, to NLO, related by

$$a_s(M^2) = a_s(R^2)\left[1+\beta_0 a_s(R^2)\ln\left(\frac{R^2}{M^2}\right)\right]. \quad (20)$$

In fact, one can resum the terms in front of the LO splitting functions, P_0^N, in eq. (19) using the relation (20). Thus to NLO accuracy the parton densities can be expressed as a function of a single scale.

The structure functions $F^N(Q^2)$ are represented by the solution of eq. (19) convoluted with the coefficient functions according to

$$F^N(Q^2) = \left[1 + a_s(R^2)c_{1,q}^N\right] f^N(Q^2,R^2)\,. \quad (21)$$

For the study of the renormalization scale dependence we identify the mass factorization scale $M^2 = Q^2$.

The factorization scale dependence of the structure function F^N is described by

$$F^N(Q^2) = \left[1 + a_s(M^2)\left(c_{1,q}^N + P_0^N \ln\left(\frac{Q^2}{M^2}\right)\right)\right] f^N(M^2)\,, \quad (22)$$

where f^N is the solution of

$$\frac{\partial f^N(M^2)}{\partial \ln M^2} = a_s(M^2)\left[P_0^N + a_s(M^2)P_1^N\right] f^N(M^2). \quad (23)$$

Here the renormalization scale is fixed by $R^2 = M^2$.

Eqs. (21) and (22) are independent of the choices of the scales R and M, respectively, up to NLO. A further improvement of the scale stability, up to $O(\alpha_s^3)$, can be obtained extending the above analysis to 3–loop order, if the corresponding splitting functions become available. To derive an estimate of the quantitative importance of the present scale dependences, R^2 and M^2 will be varied in the range between $Q^2/4$ and $4Q^2$ in Section 4.

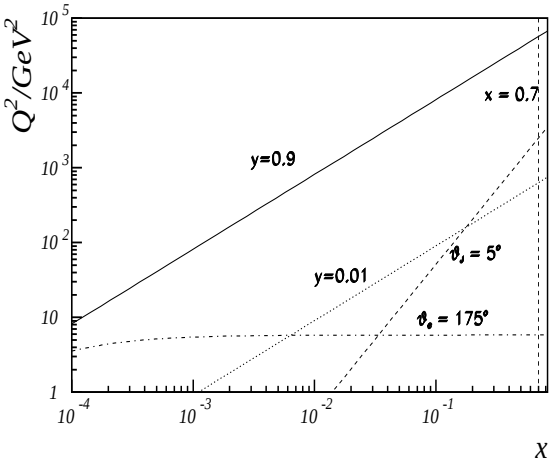

Figure 3: The kinematic range for DIS measurements at HERA used for the determination of the theoretical uncertainties of $\alpha_s(M_Z^2)$ in Section 4.

4. Estimation of the Theoretical Error $\Delta\alpha_s(M_Z^2)$

The necessity of using perturbative solutions of the renormalization group equations in representing the observables implies theoretical errors in the determination of α_s in all experimental analyses. It is convenient to compare them at a common reference scale for which we choose $\mu^2 = M_Z^2$. Furthermore we refer to the $\overline{\rm MS}$ renormalization scheme below. Recent α_s measurements were compiled in [15,16]. The most precise results obtained show that the values of $\alpha_s(M_Z^2)$ as determined in deep inelastic scattering and in e^+e^- annihilation seem to differ. The central value determined by the DIS data is [16]

$$\alpha_s(M_Z^2) = 0.112 \pm 0.004, \quad (24)$$

whereas in the e^+e^- experiments

$$\alpha_s(M_Z^2) = 0.121 \pm 0.004 \quad (25)$$

is obtained. Future high statistics measurements of α_s from deep inelastic scattering at HERA may help to resolve this difference. For the interpretation of the data, a careful treatment of the theoretical errors is required. In the following we study possible sources of theoretical uncertainty in the framework of the NLO evolution. They include:

1) The effect arising from the different representations of α_s given in eqs. (4) and (5).

2) The offsets originating in the different NLO prescriptions **(A)**–**(C)**, respectively based upon eqs. (1), (9) and (10), for the structure function evolution.

3) The theoretical uncertainties due to the freedom of choice for the renormalization and mass factorization scales.

To gauge the effect of each source of uncertainty, a reference data set was constructed for which the different displacements were measured using the χ^2 method in the kinematic regime of HERA. The different cuts used are illustrated in figure 3. The value of $\alpha_s(M_Z^2)$ was taken to be 0.112 fixing $N_f = 4$ in the entire range of Q^2, taking prescription **(A)** for the evolution, and using eq. (5) for the description of $a_s(Q^2)$.

As outlined in Section 2 the solution of the evolution equations either using eq. (1) or eq. (9) lead to different results. In the determination of $\alpha_s(M_Z^2)$ a relative shift about 0.003 is implied comparing both approaches. A similar difference has been observed between various fits in the analysis of the BCDMS $F_2^{\rm NS}$ data [17], see Table 1.

The use of either the representation for a_s as given in eq. (5) or the complete solution induces a shift of $\Delta\alpha_s(M_Z^2)$ of 0.001 or less. A much smaller difference of 0.0001 in $\alpha_s(M_Z^2)$ is obtained comparing fits using a fully iterative solution (9) of the evolution equation with one based on the expansion (10).

The largest contributions to the theoretical error of $\alpha_s(M_Z^2)$ are due to the renormalization and factorization scale uncertainties. In the present analysis, we vary each scale separately in the range $Q^2/4$ to $4Q^2$. The effects are particularly strong if no further cuts on Q^2 are applied, see Table 2. If only the Q^2 range above 50 GeV^2 is considered, the factorization scale variation in the above range results in $\Delta\alpha_s(M_Z^2)|_M = \pm 0.003$, while the corresponding error for the renormalization scale variation is estimated to be $\Delta\alpha_s(M_Z^2)|_R = {}^{+0.004}_{-0.006}$.

5. Conclusions

Various prescriptions for the NLO evolution of DIS structure functions have been discussed, and their quantitative differences were studied. The resulting *theoretical* uncertainties are rather large. At $x \simeq 10^{-4}$, e.g., the spread reaches about 6% for the proton structure function $F_2(x, Q^2)$ for identical inputs. A shift of the central value of $\alpha_s(M_Z^2)$ by about 0.003 is observed, when the same data in the HERA kinematic region are fitted with programs using the most differing prescriptions. This is to be contrasted to the offsets induced by the various *numerical* procedures. They are under control between five independent implementations [6,7,9,11,14] of $F_2(x, Q^2)$ at the level of 0.02%, see ref. [10].

The dependence of the evolution of $F_2(x, Q^2)$ on the choice of the renormalization and mass factorization scales R and M has been investigated. By varying both scales independently within the range $Q^2/4$ to $4Q^2$, the theoretical error $\Delta\alpha_s(M_Z^2)$ of future high statistics α_s measurements from F_2 scaling violations at HERA has been estimated. If a Q^2 cut of 50 GeV^2 is applied, at NLO it amounts to

$$\Delta\alpha_s(M_Z^2) = \left.\begin{matrix} +0.004 \\ -0.006 \end{matrix}\right|_R \left.\begin{matrix} -0.003 \\ +0.003 \end{matrix}\right|_M .$$

A significant reduction of the theoretical uncertainties can be expected if the presently unknown 3–loop splitting functions become available.

Acknowledgements : This work was supported on part by the EC Network 'Human Capital and Mobility' under contract No. CHRX–CT923–0004 and by the German Federal Ministry for Research and Technology (BMBF) under No. 05 7WZ91P (0).

Program	$\Lambda_{\overline{\rm MS}}$/MeV, $N_f = 4$	$\alpha_s(M_Z^2)$	χ^2/d.o.f.
Krivokhizhin *et al.* [18]	231 ± 20	0.1115 ± 0.0015	176/152
Virchaux, Ouraou [5]	235 ± 20	0.1118 ± 0.0015	178/150
González-Arroyo *et al.* [19]	220 ± 20	0.1107 ± 0.0016	180/151
Abbott *et al.* [20]	233 ± 20	0.1117 ± 0.0016	198/151
Furmanski, Petronzio [21]	270 ± 25	0.1144 ± 0.0016	181/152

Table 1: Comparison of the QCD scale parameter $\Lambda_{\overline{\rm MS}}$ obtained from NLO fits to the BCDMS $F_2^{\rm NS}$ data employing different evolution programs, taken from ref. [17]. The resulting values for $\alpha_s(M_Z^2)$ have been computed, using eq. (5) and a bottom threshold of $m_b = 4.5$ GeV.

Cut (GeV^2)	$M^2 = Q^2/4$	$M^2 = Q^2/2$	$M^2 = 2Q^2$	$M^2 = 4Q^2$
4	–	–	-0.0068	-0.012
20	$+0.0067$	$+0.0029$	-0.0024	-0.0044
50	$+0.0032$	$+0.0015$	-0.0015	-0.0029
Cut (GeV^2)	$R^2 = Q^2/4$	$R^2 = Q^2/2$	$R^2 = 2Q^2$	$R^2 = 4Q^2$
4	-0.0076	-0.0037	$+0.0032$	$+0.0059$
20	-0.0067	-0.0032	$+0.0027$	$+0.0049$
50	-0.0061	-0.0028	$+0.0023$	$+0.0042$
Cut (GeV^2)	**(B)**, eq. (9)	**(C)**, eq. (10)	α_s, eq. (4)	
4	-0.0027	-0.0001	$+0.0010$	
20	-0.0025	-0.0001	$+0.0009$	
50	-0.0023	-0.0001	$+0.0008$	

Table 2: The theoretical shifts on $\alpha_s(M_Z^2)$, from scale variations as well as from different NLO evolution and α_s prescriptions, for F_2 data in the HERA kinematic range (see Figure 3). The reference data set was generated using prescription **(A)** for the evolution equations, eq. (5) for α_s, and imposing $M^2 = R^2 = Q^2$.

REFERENCES

1. J. Blümlein, G. Ingelman, M. Klein, and R. Rückl, Z. Phys. **C45** (1990) 501, and references therein.
2. M. Botje et al., in: Proceedings of the 1996 HERA Physics Workshop, to appear.
3. D. Duke and R. Roberts, Phys. Rep. **120** (1985) 275.
4. See e.g. J. Blümlein, Surv. High Energy Physics **7** (1994) 181, in ref. [48].
5. M. Virchaux and A. Ouraou, DPhPE 87–15; M. Virchaux, Thèse, Université Paris-7 (1988);
   A. Ourau, Thèse, Université Paris-11 (1988).
6. M. Botje, QCDNUM15: A fast QCD evolution Program, to appear.
7. C. Pascaud and F. Zomer, H1 Note: `H1-11/94-404`.
8. M. Diemoz, F. Ferroni, E. Longo, and G. Martinelli, Z. Phys. **C39** (1988) 21.
9. M. Glück, E. Reya and A. Vogt, Z. Phys. **C50** (1990) 471.
10. J. Blümlein, M. Botje, C. Pascaud, S. Riemersma, W. van Neerven, A. Vogt, and F. Zomer, in: Proceedings of the 1996 HERA Physics Workshop, to appear.
11. S. Riemersma, unpublished.
12. W. Furmanski and R. Petronzio, Z. Phys. **C11** (1982) 293.
13. W. van Neerven and E. Zijlstra, Phys. Lett. **B272** (1991) 127;
    E. Zijlstra and W. van Neerven, Phys. Lett. **B273** (1991) 476; Phys. Lett. **B287** (1992) 377; Nucl. Phys. **B383** (1992) 525.
14. W. van Neerven and J. Blümlein, unpublished.
15. S. Bethke, XXXth Recontres de Moriond: QCD and High-Energy Interactions, ed. J. Tran Thanh Van, (Elsevier, Paris, 1996) p. 213.
16. J. Blümlein, Proceedings of the XXV International Symposium on Multiparticle Dynamics, Stara Lesna, Slovakia, Sep. 1995, eds. D. Brucko, L. Sandor, and J. Urban, (World Scientific, Singapore, 1996), p. 107, DESY-95-241, `hep-ph/9512272`.
17. A.C. Benvenuti et al., BCDMS collaboration, Phys. Lett. **B195** (1987) 97.
18. V. Krivokhizhin et al., Z. Phys. **C36** (1987) 51.
19. A. González–Arroyo, C. López, and F.J. Ynduráin, Nucl. Phys. **B153** (1979) 161; **B159** (1979) 515.
20. L.F. Abbott, W.R. Atwood, and R.M. Barnett, Phys. Rev. **D22** (1980) 582.
21. W. Furmanski and R. Petronzio, Nucl. Phys. **B195** (1982) 237.